



Pliocene episodic exhumation and the significance of the Muniari thrust in the northwestern Himalaya



Konstanze Stübner^{a,b,d,*}, Djordje Grujic^c, István Dunkl^b, Rasmus Thiede^d, Patricia Eugster^d

^a Department of Geosciences, Eberhard Karls Universität Tübingen, 72074 Tübingen, Germany

^b Sedimentology and Environmental Geology, Geoscience Center, University of Göttingen, 37077 Göttingen, Germany

^c Department of Earth Sciences, Dalhousie University, Halifax, NS, B3H 4J1 Canada

^d Institute of Earth and Environmental Sciences, University of Potsdam, 14476 Potsdam, Germany

ARTICLE INFO

Article history:

Received 11 April 2017

Received in revised form 13 October 2017

Accepted 16 October 2017

Available online xxxx

Editor: A. Yin

Keywords:

Himalaya

Himachal Pradesh

Muniari thrust

thermochronology

thermokinematic modelling

Pliocene

ABSTRACT

The Himalayan thrust belt comprises three in-sequence foreland-propagating orogen-scale faults, the Main Central thrust, the Main Boundary thrust, and the Main Frontal thrust. Recently, the Muniari–Ramgarh–Shumar thrust system has been recognized as an additional, potentially orogen-scale shear zone in the proximal footwall of the Main Central thrust. The timing of the Muniari, Ramgarh, and Shumar thrusts and their role in Himalayan tectonics are disputed. We present 31 new zircon (U–Th)/He ages from a profile across the central Himachal Himalaya in the Beas River area. Within a ~40 km wide belt northeast of the Kullu–Larji–Rampur window, ages ranging from 2.4 ± 0.4 Ma to 5.4 ± 0.9 Ma constrain a distinct episode of rapid Pliocene to Present exhumation; north and south of this belt, zircon (U–Th)/He ages are older (7.0 ± 0.7 Ma to 42.2 ± 2.1 Ma). We attribute the Pliocene rapid exhumation episode to basal accretion to the Himalayan thrust belt and duplex formation in the Lesser Himalayan sequence including initiation of the Muniari thrust. Pecube thermokinematic modelling suggests exhumation rates of ~2–3 mm/yr from 4–7 to 0 Ma above the duplex contrasting with lower (<0.3 mm/yr) middle-late Miocene exhumation rates. The Muniari thrust terminates laterally in central Himachal Pradesh. In the NW Indian Himalaya, the Main Central thrust zone comprises the sheared basal sections of the Greater Himalayan sequence and the mylonitic ‘Bajaura nappe’ of Lesser Himalayan affinity. We correlate the Bajaura unit with the Ramgarh thrust sheet in Nepal based on similar lithologies and the middle Miocene age of deformation. The Muniari thrust in the central Himachal Himalaya is several Myr younger than deformation in the Bajaura and Ramgarh thrust sheets. Our results illustrate the complex and segmented nature of the Muniari–Ramgarh–Shumar thrust system.

© 2017 Elsevier B.V. All rights reserved.

1. Introduction

The evolution of the Himalayan orogeny since the early Miocene has traditionally been described as the in-sequence growth and propagation towards its foreland, with progressive southward activation of the main thrusts, the Main Central Thrust (MCT), Main Boundary Thrust (MBT), and the Main Frontal Thrust (MFT; Fig. 1A). There is growing evidence that the lithotectonic units bounded by these shear zones and faults are not single crustal slices but have undergone both in- and out-of-sequence growth (e.g., Hollister and Grujic, 2006; Montomoli et al., 2015;

Pearson and DeCelles, 2005). It has been known that the Lesser Himalayan sequence (LHS), bounded by the MCT above and the MBT at the bottom, is a structurally complex tectonic unit. The upper part contains Mid-Proterozoic metasediments and granitoids and has undergone greenschist and higher grade metamorphism. The lower unit preserves the original bedding permitting mapping of numerous horses stacked in different styles of duplexes. The boundary between the two are the Muniari (MT), Ramgarh, and Shumar thrusts in the western, central, and eastern Himalaya, respectively, which may be a continuous orogen-scale structure (RMT, Pearson and DeCelles, 2005; Robinson and Pearson, 2013). Although most geologists agree on the existence of LHS duplexes, there is no agreement on their time of formation, on the significance of the RMT thrusts, or on the relative timing of deformation (i.e., the sequence of MCT–RMT–MBT; inset in Fig. 1A). In cross section restorations, the RMT is

* Corresponding author at: Institute of Earth and Environmental Sciences, University of Potsdam, 14476 Potsdam, Germany.

E-mail address: konstanze.stuebner@uni-potsdam.de (K. Stübner).

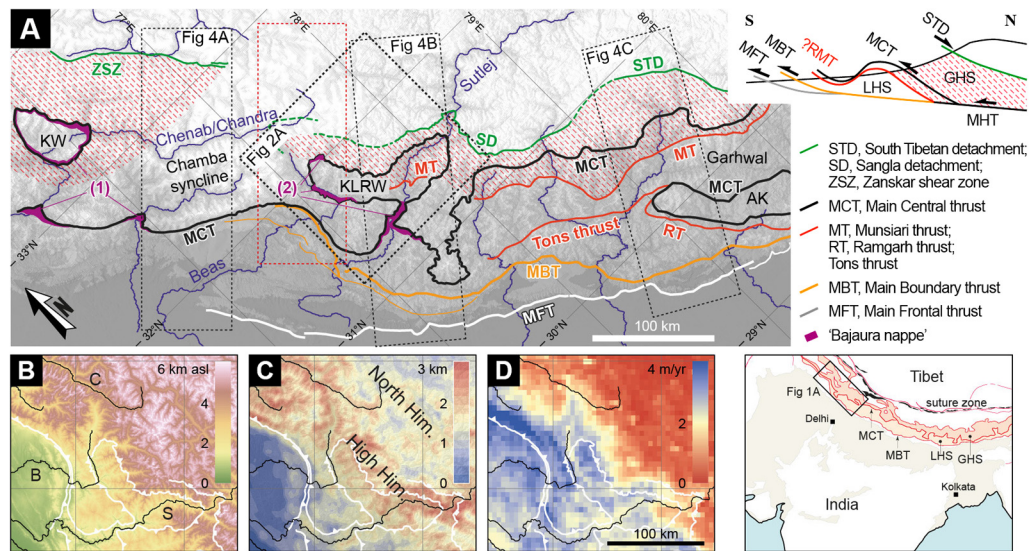


Fig. 1. (A) Tectonic overview of the NW Indian Himalaya (see overview map lower right for location; after [Srivastava and Mitra, 1994](#); [Steck, 2003](#)). Black boxes outline study area ([Fig. 2A](#)) and cross sections ([Figs. 4A–C](#)). Red box outlines Pecube model area. Note the sequence of graphitic schists and mylonitic augen gneiss mapped in the Kishtwar area (1) and in the Beas area (Bajaura nappe, 2). Hatched area outlines the approximate extent of amphibolite facies metamorphic rocks. Schematic cross section in the upper right shows the main tectonic boundaries (LHS, Lesser Himalayan sequence; GHS, Greater Himalayan sequence). A question mark is added to the Ramgarh–Munsiari thrust system (RMT) to indicate that geometries and correlations of these faults vary along the orogen and are disputed (see text and [Figs. 4A–C](#)). Further abbreviations are: KW, Kishtwar window; KLRW, Kullu–Larji–Rampur window; AK, Almora klippe. (B) Topography, (C) local relief over a radius of 4.5 km, and (D) calibrated mean annual precipitation (based on TRMM 2B31; [Bookhagen and Burbank, 2010](#)) in central and eastern Himachal Pradesh. Outline of [Figs. 1B–D](#) corresponds approximately to [Fig. 2A](#). Rivers are C – Chandra/Chenab, B – Beas, S – Sutlej. The physiographic subdivision into North Himalaya and High Himalaya is indicated in (C). (For interpretation of the references to colour in this figure legend, the reader is referred to the web version of this article.)

a passive roof thrust of LHS duplexes and has accommodated on the order of 100 km shortening, comparable to shortening across the MCT and possibly more than the MBT ([Long et al., 2011](#); [Robinson and McQuarrie, 2012](#); [Pearson and DeCelles, 2005](#)). Other studies equate the RMT with the MCT shear zone ([Searle et al., 2008](#); [Larson and Godin, 2009](#)). Estimates of the timing of the RMT thrusts vary along the orogen. Based on structural reconstructions, early Miocene ages (~ 20 – 15 Ma) have been suggested for western Nepal and eastern Bhutan ([Long et al., 2011](#); [Robinson and McQuarrie, 2012](#)). Younger ages have been suggested for Nepal (~ 15 – 11 Ma, [Pearson and DeCelles, 2005](#); ~ 11 – 9 Ma, [Kohn et al., 2004](#)) and for eastern Himachal Pradesh (~ 10 – 0 Ma, [Vannay et al., 2004](#) or ~ 10 – 6 Ma, [Caddick et al., 2007](#)). These differences may result from the different approaches to constraining the age of movement on a fault (e.g., thermochronological ages, structural reconstructions) or from the inconsistent definition of the thrust(s) and the resulting difficulties in along-strike correlation.

To investigate the geometry and kinematics of the Munsiari thrust in the northwest Indian Himalaya, we mapped a transect from LHS rocks in the western Kullu–Larji–Rampur window (KLRW), central Himachal Pradesh, into the Greater Himalayan sequence (GHS) in the MCT hanging wall. We constrain cooling and exhumation histories by new zircon (U–Th)/He (ZHe) ages from this transect and from the central Himachal GHS and integrate this new dataset with previously published data. Using Pecube thermokinematic modelling, we scrutinize the episodic Neogene exhumation histories and unravel the contributions of different tectonic phases on the evolution of the NW Himalaya.

2. Geological background

In Himachal Pradesh, the MCT separates Neoproterozoic to Cambrian meta-greywacke (Haimanta formation) with early Paleozoic granite intrusions from LHS orthogneisses and metasediments (e.g., [Frank et al., 1995](#); [Fig. 2A](#)). The Haimanta rocks are mostly greenschist facies to unmetamorphosed; amphibolite-facies rocks

are exposed in the valleys of the upper Beas, Tosh, and Chandra Rivers ([Epard et al., 1995](#); [Wyss, 2000](#)) and in eastern Himachal Pradesh (Sutlej River section; [Fig. 2A](#)). In the Sutlej section, the Sangla detachment correlates with the STD. In the Beas section, presence and location of the STD are disputed, and the lower-grade Haimantas are attributed either to the GHS (e.g., [Steck, 2003](#)) or to the Tethyan Himalayan sequence (e.g., [Webb et al., 2011](#)). The KLRW exposes the MCT ≥ 100 km northeast of its frontal trace. The LHS in the window comprises Paleoproterozoic quartzite (Berinag formation) and Wangtu orthogneiss (~ 1.8 Ga deposition and emplacement ages; [Miller et al., 2000](#); [Fig. 2A](#)). The MCT shear zone is several 10s to 100s meters thick. It comprises mylonitic orthogneiss (Baragaon augen gneiss) with the same magmatic age and isotopic composition as the Wangtu orthogneiss ([Thöni, 1977](#); [Frank et al., 1995](#)), graphitic schists and phyllites and, locally, dark limestone bands (e.g., [Stephenson, 1997](#); own observations). In the NW Indian Himalaya including the KLRW and Kishtwar window, the sequence of augen gneiss and graphitic schists is referred to as ‘Bajaura nappe’ or ‘Lower crystalline nappe’. It is either attributed to the MCT shear zone (e.g., [Thöni, 1977](#); [Frank et al., 1995](#); [Stephenson et al., 2001](#)) or interpreted as a separate unit (e.g., [Steck, 2003](#); [Webb, 2013](#); [Fig. 1A](#)).

The NW Himalayan MCT was active from the latest Oligocene–early Miocene to the middle Miocene ([Vannay et al., 2004](#); [Roby et al., 2006](#)). Rapid exhumation of the metamorphic GHS from mid-crustal depths (peak pressures ~ 5 – 9 kbar) is reflected, for example, in ~ 20 – 21 Ma muscovite $^{40}\text{Ar}/^{39}\text{Ar}$ (MAR) ages in the Beas and Chandra valleys ([Schlup et al., 2011](#); [Stübner et al., 2014, 2017](#)); slightly younger MAR ages in the Sutlej GHS (~ 15 – 17 Ma; [Vannay et al., 2004](#)) could be related to the enhanced fluvial incision of the Sutlej river, which led to an estimated ~ 10 km of additional erosion compared to the Beas section ([Thiede et al., 2005](#)).

The MT is mapped in the Sutlej section as the mylonitic base of a ~ 16 km thick amphibolite-facies, pervasively top-to-the-SW sheared sequence of paragneiss and Wangtu orthogneiss (Lesser Himalayan crystalline, LHC; [Vannay and Grasmann, 2001](#)). Monazite U, Th–Pb and garnet Sm–Nd ages (~ 6 – 11 Ma) and MAR

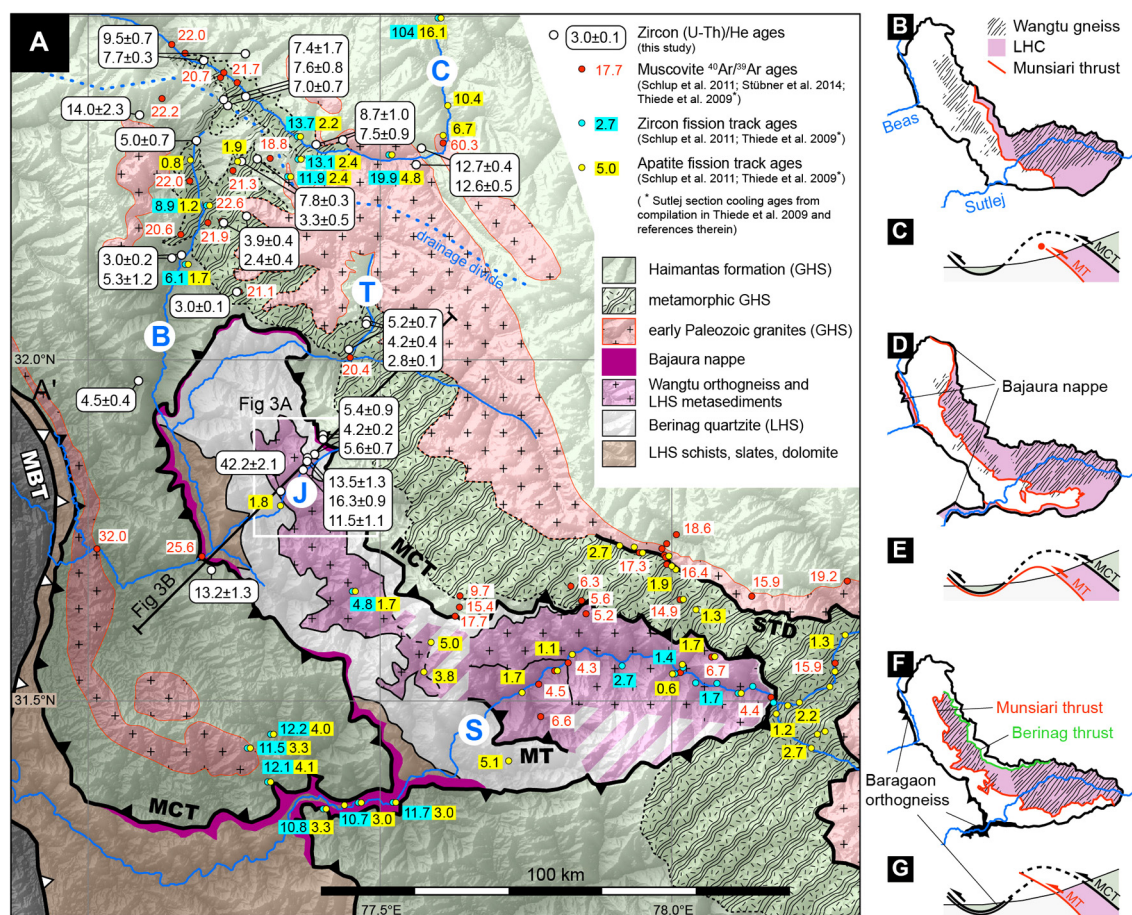


Fig. 2. Geology of central Himachal Pradesh and different tectonic models for the Kullu-Larji-Rampur window and Munsiri thrust. (A) Map (after Jain and Anand, 1988; Steck, 2003; Webb et al., 2011, and own mapping) with new zircon (U-Th)/He ages and apatite and zircon fission-track and muscovite $^{40}\text{Ar}/^{39}\text{Ar}$ ages compiled from the literature (Schlup et al., 2011; Stübner et al., 2014, 2017; Thiede et al., 2009 and references therein; see also Supplementary Table S2). Bold blue letters label the rivers referred to in the text: C, Chandra; B, Beas; T, Tosh; J, Jiwa; S, Sutlej River. Locations of detailed map and cross section of the Jiwa section (Figs. 3A–B) are indicated. Sketches on the right side show maps of the window and implicit models for the MCT and MT after (B, C) Vannay and Grasmann (2001); (D, E) Steck (2003); (F, G) simplified after Webb (2013). Note that in Webb (2013), the MT is one thrust in a Pliocene antiformal stack with at least 6 horses. Exposure of Wangtu orthogneiss in all maps after Jain and Anand (1988). (For interpretation of the references to colour in this figure legend, the reader is referred to the web version of this article.)

ages (~4–5 Ma) from the LHC document middle-late Miocene prograde metamorphism followed by rapid decompression and cooling ('hairpin' metamorphic path) in the late Miocene and early Pliocene accommodated by SW-directed thrusting on the MT (e.g., Vannay et al., 2004; Caddick et al., 2007). Away from the Sutlej River, the lithologies and structures in the window are disputed. For example, the southernmost exposure has been interpreted as paragneiss or orthogneiss and may correlate with the LHC or LHS (cf. Figs. 2B, 2D, 2F). Outcrops of Wangtu orthogneiss in the Sutlej section and in the northwestern window may be separated by exposure of Berinag quartzite (Jain and Anand, 1988; Fig. 2B) or form a continuous body (e.g., Steck, 2003; Webb et al., 2011; Figs. 2D, 2F). In particular, disputed intersection relationships between the MT and MCT have important implications on the interaction of these faults: If the KLRW antiform is a fault-propagation fold above the tip of the MT (Vannay and Grasmann, 2001; Fig. 2C), displacement on the MT is limited to the amplitude of the KLRW antiform (~ a few kilometres). Alternatively, correlation of the Bajaura nappe northeast and southwest of the window with the LHC suggests that both the MT and the MCT are folded within the KLRW, e.g., as a result of a deeper blind thrust (Steck, 2003; Fig. 2D–E). Webb et al. (2011) interpret the MT as an out-of-sequence thrust that cuts the MCT southeast of the Sutlej River. Fig. 2G shows a simplified version of their model, which depicts the rocks in the KLRW as an antiformal stack of multiple horses; here, the MT is one of several thrusts within the duplex (Webb, 2013). The inter-

pretation of the KLRW antiform and window as resulting from MT thrusting implies a late Miocene (Caddick et al., 2007) to Pliocene formation age (Vannay et al., 2004; Thiede et al., 2005), whereas Jain et al. (2000) propose a Pleistocene age of window formation.

3. Field mapping and zircon (U-Th)/He thermochronology

We mapped the disputed western part of the window along the Jiwa River (Figs. 2A, 3). The Berinag formation consists of massive quartzite and minor phyllite with poorly developed bedding; foliation dips to the NE to NNE. The contact to the overlying Wangtu orthogneiss is not exposed but could be located to <50 m. The ~4 km thick sequence of Wangtu orthogneiss is strongly deformed by pervasive top-to-the-SSW shear and includes ubiquitous phyllonites and L-tectonites. Gneissic foliation dips ~30–50° to the NNE, lineation plunges down-dip. It is overlain by ~1 km white massive quartzite; the contact between these units is not exposed.

The MCT shear zone consists of 500–1000 m thick black graphitic schists and phyllites capped by protomylonitic augen gneiss. The lower contact to the Berinag quartzite is sharp and undulating on length scales of ~5–50 m. The phyllitic sequence has a wavy foliation, numerous shear bands with variable orientation and shear sense, and meter-to-10 m scale tight to isoclinal folds; the fabric is crosscut by subvertical quartz veins. The augen gneiss has a strong S–C' fabric indicating top-to-the-SSW shear. Above the augen gneiss, the Haimanta metagreywacke consists of 10 cm to

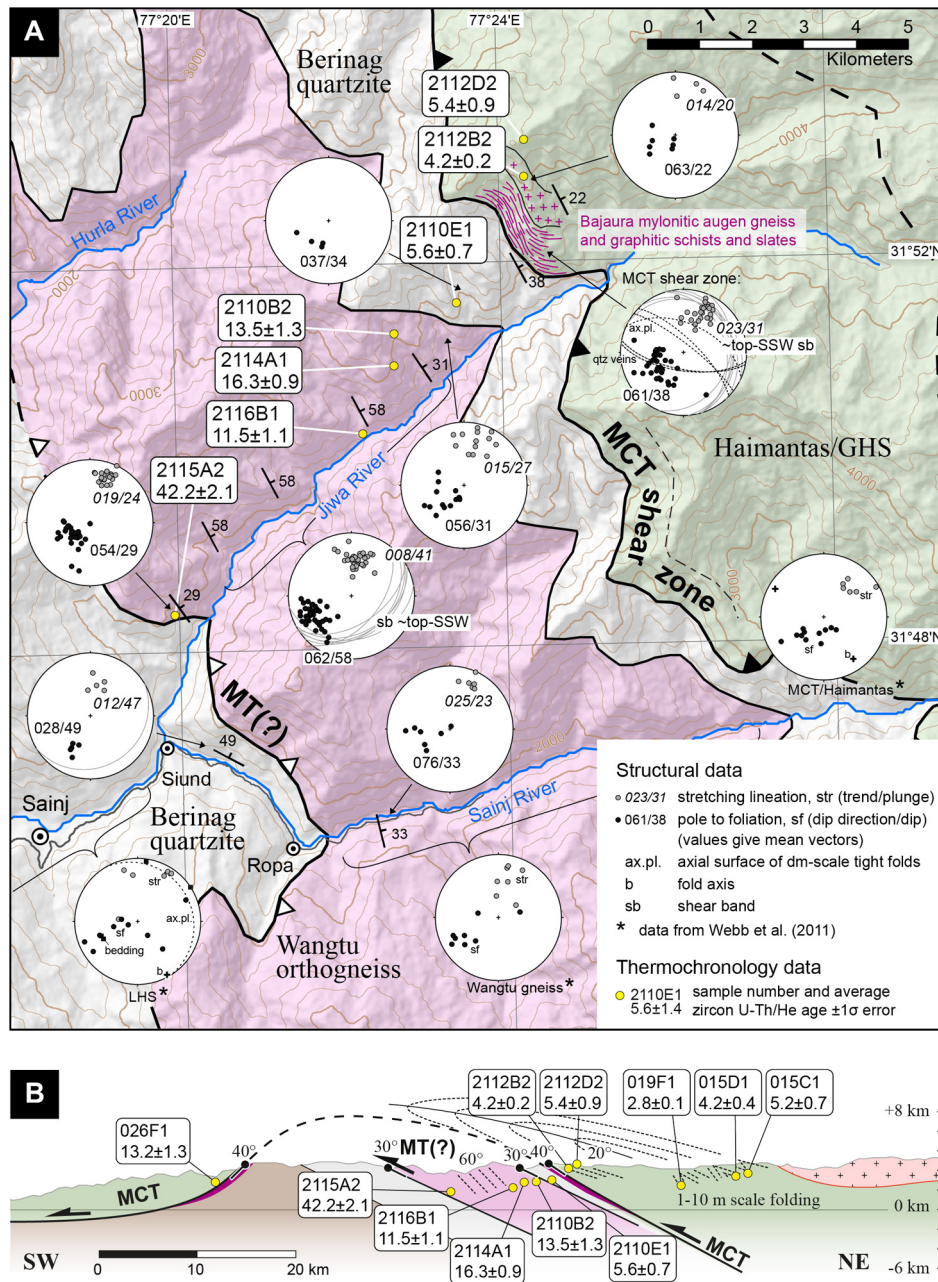


Fig. 3. (A) Map and structural data from the Jiwa River section in the western Kullu–Larji–Rampur window. Note the succession of graphitic slates and schists overlain by protomylonitic augen gneiss at the base of the Haimanta metasedimentary sequence, which we correlate with the Bajaura unit described in the northern, western, and southwestern window margin. Here, we attribute the Bajaura unit to the MCT shear zone. The Munsiri thrust was not unambiguously identified in this study; here it is shown at the base of the Wangtu orthogneiss (cf. Webb et al., 2011; see text for alternative scenarios). (B) Cross section across the western window (see Fig. 2A for location and legend). Tad poles and dashed lines indicate the projected dip of the structures. Recumbent SW-vergent folding of the GHS northeast of the window (e.g., Wyss, 2000) is shown schematically. Note the transition from mid-Miocene to Pliocene ZHe ages across the contact between Wangtu gneiss and overlying Berinag quartzite.

several meters thick layers of quartz-feldspar rich lithologies and thin bands of garnet mica schist (~2–5 cm). The layering probably reflects bedding compositional changes. Foliation is subparallel to layering. A weak S–C' fabric is locally developed in garnet mica schists.

We analysed ZHe ages from seven samples along the Jiwa section and 24 samples from the frontal GHS west of the window and the greenschist to amphibolite-grade GHS in the Tosh, Beas, and Chandra valleys (Figs. 2A and 3). Reported ages are sample mean ages $\pm 1\sigma$ standard deviation of the mean calculated from 3–5 single-grain aliquots per sample (see Supplementary Materials for analytical details, sample locations, and results). In the Jiwa section, samples from the Wangtu orthogneiss yielded ages

of 11.5 ± 1.1 to 42.2 ± 2.1 Ma. Samples from the overlying Berinag quartzite, the augen gneiss, and the GHS yielded 4.2 ± 0.2 to 5.6 ± 0.9 Ma. This younger age group is similar to ZHe ages from the Tosh and Beas GHS (mostly 2.4 ± 0.4 to 5.3 ± 1.2 Ma; Fig. 2A). ZHe ages from the Chandra valley and from two samples in the northwestern and the frontal GHS are older (7.0 ± 0.7 to 14.0 ± 2.3 Ma). A compilation of thermochronological ages from central Himachal Pradesh (MAR, ZHe, apatite and zircon fission track ages (AFT, ZFT); Schlup et al., 2011; Stübner et al., 2014; see Supplementary Table S2) reveals two first-order trends (Fig. 2A): (1) The youngest ages of each thermochronometer are obtained from the Tosh and upper Beas valleys from an area that corresponds approximately to the amphibolite-facies GHS. We will refer

to this region as the Beas/Tosh GHS. (2) Cooling ages in the Chandra valley are slightly older than those from the Beas/Tosh GHS and increase over short distances towards the north. This northward increase in cooling ages across the Beas–Chandra drainage divide corresponds to the transition from the deeply dissected, steep ranges of the ‘High Himalaya’ to the highlands of the ‘North Himalaya’ and coincides with a ~ 10 -fold northward decrease in mean annual precipitation across the drainage divide (Bookhagen and Burbank, 2010; Figs. 1C–D). Our study focuses on the exhumation history of the High Himalaya and, in particular, the cause of the Pliocene ZHe ages in the Beas/Tosh GHS. The narrowly defined MAr (~ 20 – 21 Ma) and ZHe (~ 3 – 5 Ma) ages, the ~ 15 Myr gap between these ages, and the wider spread in ZFT ages document an episodic cooling history with rapid cooling in the early Miocene and Pliocene, similar to the cooling histories documented in the eastern Himachal and Garhwal Himalaya (Thiede et al., 2009). The spatial confinement of the young ZHe ages to the Beas/Tosh GHS, the lack of an obvious topographic control on this exhumation (e.g., the region of young ZHe ages does not correspond to locally higher relief; Fig. 1C), and the abrupt southward increase in ZHe ages along the Jiwa section suggest a tectonic control on the Pliocene exhumation episode. This interpretation contrasts with Thiede et al. (2009), who attribute a belt of Pliocene AFT ages along the southern slopes of the Himachal and Garhwal Himalaya to climatically controlled rapid erosion.

4. Tectonic interpretation and discussion

The sequence of graphitic schists overlain by mylonitic augen gneiss at the base of the Haimanta metasediments in the Jiwa section is remarkably similar to the Bajaura unit in the southern, western, and northern KLRW, and as in the Kishtwar window (Figs. 1A, 2A). The MT was not identified in the Jiwa section. It could be located at the base of the Wangtu orthogneiss (Fig. 2F), or locally reactivate the MCT shear zone in the Jiwa valley and disappear as a blind thrust below the High Himalaya in the Beas/Tosh area (Fig. 2B). Because the Bajaura nappe is a distinct lithotectonic unit above the Wangtu gneiss and overlying quartzite, we suggest that it is part of the MCT shear zone rather than a lateral continuity of the LHC (Fig. 2D, Stephenson et al., 2001). Both alternatives for the location of the MT in the western KLRW—below the Wangtu gneiss or coinciding with the MCT zone—imply that there is no evidence of the MT west of the KLRW and the MT thus ends laterally in central Himachal Pradesh.

The Pliocene exhumation episode documented by our ZHe ages coincides approximately with the late Miocene to Pliocene age of MT thrusting and an episode of rapid exhumation of the LHC in the Sutlej section (Vannay et al., 2004; Caddick et al., 2007). The localization of rapid Pliocene exhumation north and northeast of the western KLRW suggests that exhumation may have been driven by thrusting on the westernmost segment of the MT, which is a blind thrust below the Beas/Tosh GHS (Fig. 2B). This assumption implies that the westernmost MT is located structurally *above* the Wangtu gneiss separating Pliocene ZHe ages in the hanging wall from mid-Miocene ages in the footwall (Fig. 3). However, we speculate that a similar ZHe age pattern may result from thrusting along the *base* of the Wangtu orthogneiss and that the age contrast between Wangtu orthogneiss and overlying units reflects the different thermal histories of these units prior to the onset of Pliocene exhumation (i.e., underthrusting of the cold LHS and overthrusting and exhumation of the hot GHS along the MCT) combined with different thermal properties of the LHS and GHS (Grasemann, 1993). Testing of this hypothesis requires more thorough investigation of the thermal histories and better constraints on the thermal properties of the involved rock units. Our thermokinematic modelling suggests that the offset in ZHe ages across the contact between Wangtu gneiss

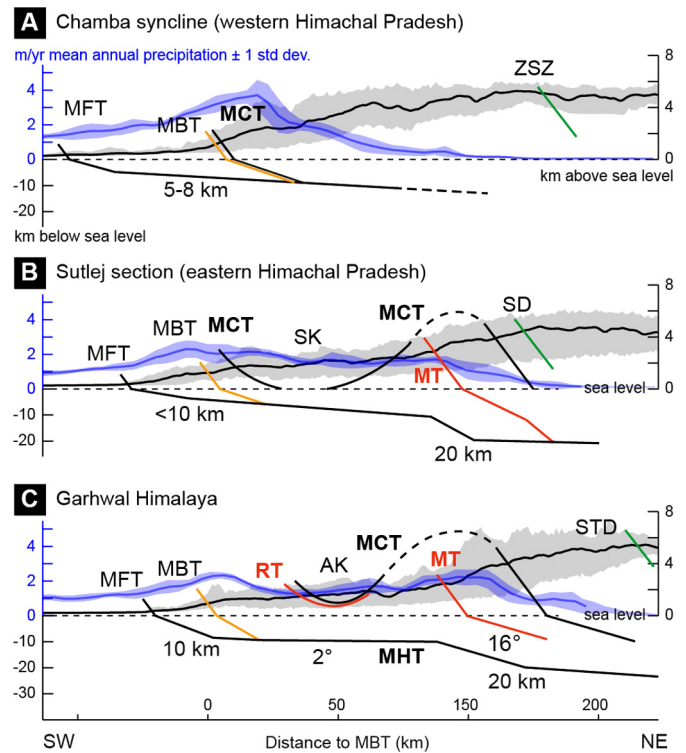


Fig. 4. Orogen-normal cross sections across the (A) western and (B) eastern Himachal, and (C) Garhwal Himalaya; profile locations are shown in Fig. 1A. Topography from ASTER data; grey bands show maximum and minimum elevations within 100 km-wide swaths. Calibrated mean annual precipitation shown as blue bands (Bookhagen and Burbank, 2010). Structures in (A) are inferred from thermochronological data (Deeken et al., 2011) and from seismic data in the Sub-Himalaya (Powers et al., 1998); (B) is from a balanced cross section reconstruction (Webb, 2013); (C) is from seismic (Caldwell et al., 2013) and structural data (Pearson and DeCelles, 2005; Mandal et al., 2014). Abbreviations see Fig. 1. (For interpretation of the references to colour in this figure legend, the reader is referred to the web version of this article.)

and Berinag quartzite may not reflect discrete fault offset but result from the rock uplift patterns above a thrust ramp at depth (see below). We conclude that our thermochronological data do not offer constraints on the geometry or location of the MT but are in general agreement with its western termination in central Himachal Pradesh.

Studies in the central and eastern Himalaya have attributed the spatially and temporally variable exhumation rates to a number of mechanisms including flat-ramp geometries and lateral ramps in the MHT (Robert et al., 2011; Coutand et al., 2014) and basal accretion and duplex formation in the LHS (Bollinger et al., 2006; Célérier et al., 2009; Herman et al., 2010). Thermokinematic modelling has demonstrated that the cooling-age record is not unique to a particular tectonic mechanism, and the distinction between the different models (i.e., MHT ramp, basal accretion, out-of-sequence thrusting) requires the knowledge of the geometry of the involved structures (e.g., Whipp et al., 2007; Herman et al., 2010). In the central and eastern Himalaya, seismic studies constrain the depth and flat-ramp geometry of the MHT (e.g., Caldwell et al., 2013 and references therein), but few constraints are available for the northwest Himalaya west of Garhwal. In the Sutlej section, cross-section balancing suggests a 6° NE-dipping MHT at 5–15 km depth southwest of the KLRW, a 15° dipping ramp and an antiformal stack of LHS and LHC horses below the window, and a flat MHT at ≥ 20 km depth below the Sutlej GHS (Fig. 4B; Webb, 2013). Because of the limitations in cross-section retro-deformation in settings with pervasive ductile deformation, and the uncertainties in the pre-deformation thicknesses of the stratigraphic units

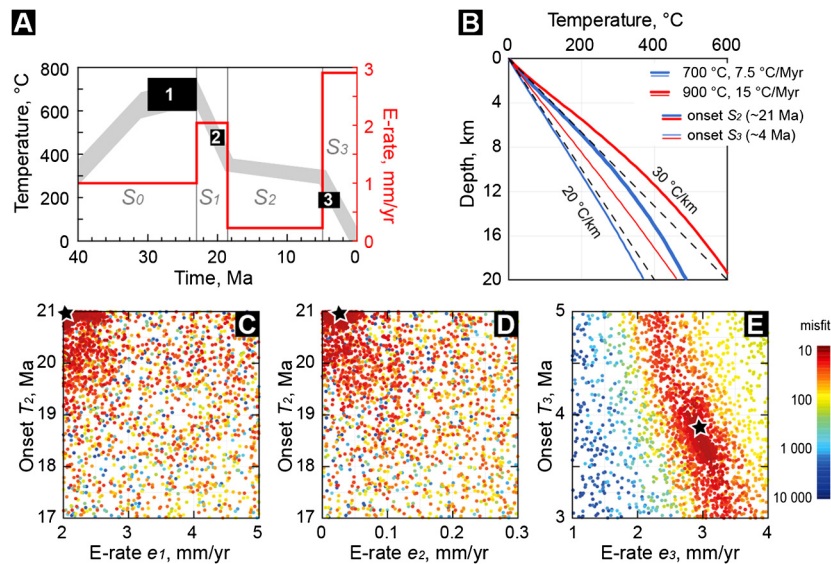


Fig. 5. (A) Schematic representation of the 1D inversion models. Black boxes represent time-temperature constraints: 1, peak temperatures 600–750 °C at 23–26 Ma; 2, ~20–21 Ma muscovite $^{40}\text{Ar}/^{39}\text{Ar}$ ages; 3, ~5–7 Ma zircon (U–Th)/He ages (see text). The thermal history is modelled as four stages (red line) with variable exhumation rates during stages S_1 – S_3 ($\dot{\epsilon}_1$, $\dot{\epsilon}_2$, $\dot{\epsilon}_3$), and variable onset of S_2 – S_3 (T_2 , T_3). (B) Geothermal gradients at the onset of stages S_2 (bold lines) and S_3 (thin lines) for a basal temperatures and heat production of 700 °C and 7.5 °C/Myr (blue; see Fig. 5C–E) and 900 °C and 15 °C/Myr (red). (C)–(E) Inversion results of the four-stage, vertical exhumation scenario for the Beas/Tosh GHS. Each dot represents a forward model colour-coded by the misfit between the model predicted and observed ages. Stars denote the lowest-misfit solution obtained in 2600 forward model runs ($\dot{\epsilon}_1 = 2$ mm/yr; $\dot{\epsilon}_2 = 0.03$ mm/yr; $\dot{\epsilon}_3 = 2.9$ mm/yr; $T_2 = 21$ Ma; $T_3 = 3.8$ Ma). (For interpretation of the references to colour in this figure legend, the reader is referred to the web version of this article.)

(including gneissic and magmatic LHS basement units), this reconstruction is probably more accurate for shallow structures such as the LHS horses than for deeper structures such as the MT or the MHT. In the Chamba area between the Kishtwar window and KLRW, Deeken et al. (2011) argue that the MHT dips at a shallow angle without a ramp or an LHS duplex below the MCT based on slow and low-magnitude Cenozoic surface denudation throughout the area (Fig. 4A); the depth of the MHT is unknown. The MBT and MCT are within a structural distance of <2 km and merge with the MHT at a frontal position (Powers et al., 1998; Thiede et al., 2017). Graphitic schists of the Bajaura unit are mapped in the MCT footwall (Fig. 1A). The Beas section is closer to the Sutlej than to the Chamba section, but several factors limit our knowledge of the geometry of the Beas thrust system: (1) As discussed above, the ductile and mid-crustal structures are poorly constrained by cross-section reconstructions in the Sutlej. (2) Enhanced and focused fluvial incision of the Sutlej locally affects the fault geometries. (3) The geometry of the MT in the Beas section is disputed.

5. Thermokinematic modelling

5.1. Model setup

In order to quantify the amount of Pliocene exhumation in the Beas/Tosh GHS, constrain the time frame of this exhumation episode, and determine Pliocene exhumation rates, we performed thermokinematic modelling using the Pecube code (Braun et al., 2012). Pecube solves the heat production, conduction, and diffusion equation for a given 3D kinematic field and thus allows to explore the effects of tectonic transport and erosion on the thermal field, on particle cooling histories, and on cooling ages. Our models build on numerous previous thermokinematic modelling studies in the Himalaya (Bollinger et al., 2006; Whipp et al., 2007; Célérier et al., 2009; Herman et al., 2010; Robert et al., 2011; Coutand et al., 2014). We took advantage of the observation that in regions of rapid material transport ($> \sim 1$ mm/yr) heat advection dominates over conduction and the models are relatively insensitive to thermal parameters and basal heat flow (Whipp et

al., 2007), and we adopted material properties within the range of values used in earlier studies (thermal diffusivity, 35 km²/Ma; heat production, 7.5–15 °C/Ma; constant basal temperature condition 700–900 °C at 40 km depth; see Supplementary Table S3 for a complete list of model parameters). We modelled lateral transport within the orogenic wedge using a 80 × 185 × 40 km (width × length × depth) model domain oriented parallel to the direction of tectonic transport, i.e. trending NE (Fig. 1A). India–Asia convergence is accommodated by the MHT, which consists of planar fault segments striking perpendicular to the model long axis (see Fig. 6A). GPS-derived shortening-rate estimates in Himachal Pradesh range from ~14 mm/yr NE (Jade et al., 2014) to ~18 mm/yr NNE (Stevens and Avouac, 2015) and are generally lower than those in the central and eastern Himalaya; shortening is assumed to be constant since at least ~10 Ma (Meigs et al., 1995). The model swath trends NE (Fig. 1A). For the purpose of modelling, total convergence of 14 mm/yr is split into underthrusting of the Indian plate below the MHT, and overthrusting, which is assumed to be compensated by denudation such that the topography remains constant throughout the model (convergence partitioning, e.g., Herman et al., 2010). Thermokinematic modelling studies in the central and eastern Himalaya suggest overthrusting velocities corresponding to 25–35% of the total convergence. The model topography is derived from an ASTER digital elevation model resampled to a resolution of 500 m. Changes in topography with time affect primarily low-temperature thermochronometer data and are not considered in this study.

The 21–20 Ma MAr ages in the Beas, Tosh, and Chandra GHS place an upper limit on the exhumation that has occurred since the early Miocene. In a first step, we approximate the Neogene exhumation history of the Beas/Tosh GHS—the region of Pliocene ZHe ages—by modelling temporally variable vertical exhumation, i.e., disregarding lateral transport. We performed four-stage exhumation models with variable timing and exhumation velocities for each time step; material properties and boundary conditions were identical to the MHT models. Stage S_0 (40 to 23 Ma at $\dot{\epsilon}_0 = 1$ mm/yr) generates a ~30 °C/km geothermal gradient representative of the metamorphic environment at the onset of early

Miocene exhumation (600–750 °C at 20–30 km, [Epard et al., 1995](#); [Wyss, 2000](#); [Fig. 5B](#)). Stages S_1 , S_2 , and S_3 model the episodic exhumation history since the early Miocene ([Fig. 5A](#)). For each set of parameters, the model predicted ages were compared to the observed MAR, ZFT, ZHe, and AFT ages (see Supplementary Table S2), and a misfit

$$\text{misfit} = \frac{1}{N} \sum_{i=1}^N \left(\frac{P_i - O_i}{\sigma_{O_i}} \right)$$

was calculated, where P_i and O_i are the predicted and observed cooling ages, σ_{O_i} is the error on the observed ages, and N is the number of observations. We used the Neighbourhood Algorithm inversion scheme of Pecube to search the parameter space for the lowest-misfit parameter set ([Fig. 5C–E](#)). Low-misfit models suggest a small amount of exhumation during stages S_1 and S_2 ([Figs. 5C–E](#)). Predictions $\dot{\epsilon}_1 = 2$ mm/yr, $\dot{\epsilon}_2 = 0.03$ mm/yr and $T_2 = 21$ Ma are limited by the parameter space, and the actual values are meaningless beyond the recognition that total exhumation during S_2 approaches 0 km. For the Pliocene exhumation stage (S_3), the total amount of exhumation is tightly constrained at 11 km. A range of exhumation rates $\dot{\epsilon}_3 \sim 2.5$ –3.5 mm/yr and $T_3 \sim 3$ –4.5 Ma produce similar low-misfit solutions; the optimal solution is $\dot{\epsilon}_3 = 2.9$ mm/yr and $T_3 = 3.8$ Ma. The best-fit values for T_3 and $\dot{\epsilon}_3$ are controlled by the upper-crustal geothermal gradient at the onset of S_3 . For the inversion in [Figs. 5C–E](#) (basal temperature 700 °C, heat production 7.5 °C/Myr) the upper-crustal thermal gradient at the onset of S_3 is ~ 20 °C/km ([Fig. 5B](#)). A basal temperature of 900 °C and heat production of 15 °C/Myr, which result in a thermal gradient of 40 °C/km at the end of early Miocene exhumation, predict a gradient of ~ 25 °C/km at the onset of S_3 and yield the best-fit solution $T_3 = 3.3$ Ma and $\dot{\epsilon}_3 = 2.7$ mm/yr (total exhumation 9 km; [Fig. 5B](#)). The predictions for duration and exhumation velocities of stages S_1 and S_2 (i.e., exhumation during S_2 approaching 0 km) are not affected by these variations in thermal parameters and boundary conditions. Additional model runs allowing S_3 to end before 0 Ma (i.e., the possibility that the rapid exhumation episode ended before the Quaternary) did not reduce the misfit.

Early Miocene exhumation of the GHS from mid-crustal depth is poorly simulated by the Pecube models because of pervasive ductile deformation during exhumation, the involvement of melt and latent heat released by melt crystallization, and retrograde metamorphic reactions. Furthermore, this stage is probably more strongly affected by lateral heat advection than the Pliocene exhumation episode. Therefore, we attach no significance to the modelled timing and exhumation rates of stages S_1 and S_2 ; the important outcome of this simulation is that middle-late Miocene exhumation rates were very low allowing the deformed isotherms to relax over 10–15 Myr. During S_2 , the underthrusting of cold Indian material probably resulted in colder geothermal gradients than predicted by the 1D simulation. On the other hand, the sedimentary rocks of the underthrust LHS may have lower thermal conductivities than the crystalline rocks of the GHS leading to an insulating effect and maintaining a hotter geotherm within the GHS than predicted by our models ([Grasemann, 1993](#); see also [Law et al., 2013](#)).

In a second step, we took into account the significant lateral material transport and designed Pecube models that simulate a belt of enhanced exhumation above a ramp in the MHT. We argued above that the Pliocene exhumation episode in the Beas/Tosh GHS may reflect rock uplift above the western termination of the MT, i.e. is the expression of out-of-sequence thrusting or fault-propagation folding. Previous studies have shown that even where extensive thermochronological data sets are available, the discrimination of different tectonic scenarios (MHT ramp, LHS

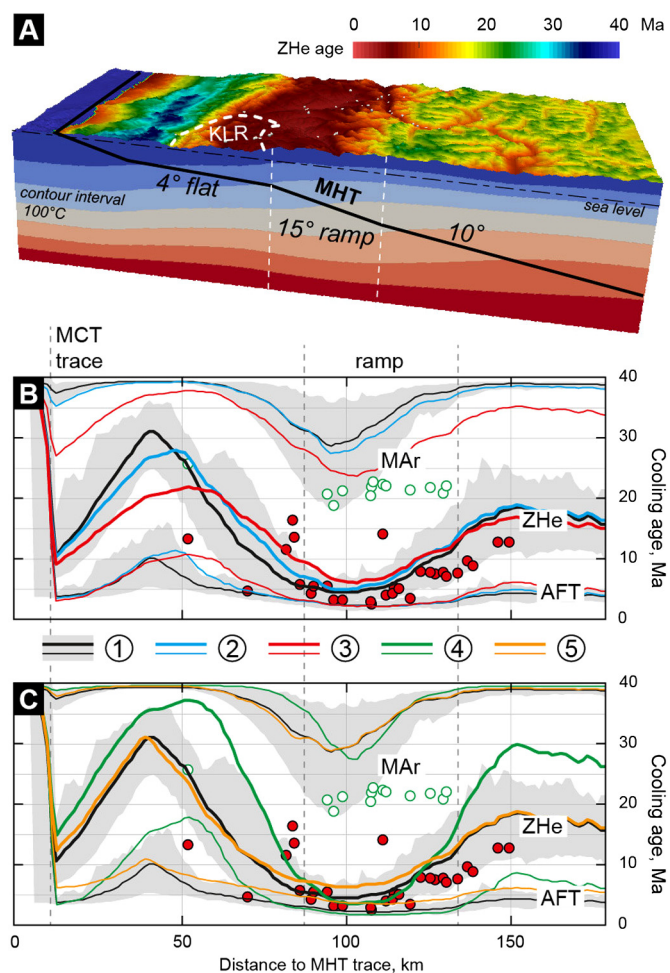


Fig. 6. (A) Pecube model output (thermal field and zircon (U–Th)/He age distribution) for a 15° dipping MHT ramp, $v_3 = 7$ mm/yr overthrusting, 7 mm/yr underthrusting, active 5.8–0 Ma; prior to ramp thrusting, constant exhumation at $\dot{\epsilon}_2 = 0.15$ mm/yr is applied 40–5.8 Ma. (B, C) Average modelled muscovite $^{40}\text{Ar}/^{39}\text{Ar}$, zircon (U–Th)/He, and apatite fission track ages versus distance to MHT trace for five different models. 1: $\dot{\epsilon}_2 = 0.15$ mm/yr, dip = 15°, $v_3 = 7$ mm/yr, $T_3 = 5.8$ Ma (same as [Fig. 6A](#); misfit = 40; grey bands indicate maximum and minimum ages). 2: $\dot{\epsilon}_2 = 0.2$ mm/yr, dip = 15°, $v_3 = 7$ mm/yr, $T_3 = 5.1$ Ma (misfit = 53). 3: $\dot{\epsilon}_2 = 0.3$ mm/yr, dip = 15°, $v_3 = 7$ mm/yr, $T_3 = 4.1$ Ma (misfit = 132). 4: $\dot{\epsilon}_2 = 0.15$ mm/yr, dip = 20°, $v_3 = 7$ mm/yr, $T_3 = 4.3$ Ma (misfit = 75). 5: $\dot{\epsilon}_2 = 0.15$ mm/yr, dip = 15°, $v_3 = 5$ mm/yr, $T_3 = 8.6$ Ma (misfit = 177). Misfit is calculated from all apatite fission track and zircon (U–Th)/He ages; the condition that all predicted muscovite $^{40}\text{Ar}/^{39}\text{Ar}$ ages are ≥ 19 Ma applies to all models. Green and red dots are observed muscovite $^{40}\text{Ar}/^{39}\text{Ar}$ and zircon (U–Th)/He ages. Dashed lines outline the extent of the ramp. (For interpretation of the references to colour in this figure legend, the reader is referred to the web version of this article.)

duplex, out-of-sequence thrust) is challenging if not impossible (e.g., [Herman et al., 2010](#)). Moreover, even if the location of the MT in the western KLRW was identified, the pattern of exhumation depends on the style and geometry of fold-propagation folding (e.g., [Allmendinger, 1998](#)). [Mercier et al. \(2017\)](#) demonstrate that the formation of duplex structures is intimately linked to the evolution of fault ramps. Therefore, we argue that a MHT ramp model is a reasonable approximation for the Pliocene exhumation episode (cf. [Célérier et al., 2009](#)).

The ramp models ([Fig. 6](#)) include a 32 km wide, 10–20° dipping ramp below the Beas/Tosh GHS designed to reproduce the band of Pliocene ZHe ages. A flat below the KLRW and frontal GHS is at 5–8 km depth, the lower flat starts at depths between 13 and 20 km. We did not simulate the early Miocene rapid exhumation because of the uncertainties discussed above. Instead, we explored a two-stage tectonic scenario (S_2 , S_3 in accordance with the 1D

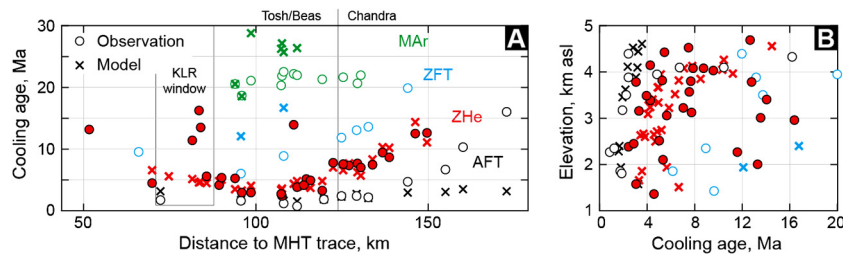


Fig. 7. Model predicted and observed cooling ages (A) as function of distance to MHT trace and (B) in an age–elevation diagram. Model ages from $\dot{\epsilon}_2 = 0.15$ mm/yr, 15° ramp, $v_3 = 7$ mm/yr, 5.8–0 Ma (see Fig. 6A).

models): In all MHT models, stage S_2 starting at 40 Ma is vertical exhumation at a constant rate that represents the combined effects of rapid early Miocene exhumation and middle-late Miocene thermal relaxation. We ran models with $\dot{\epsilon}_2 = 0.15$ to 0.3 mm/yr, the latter value representing the lower end of the range of Miocene–Pliocene exhumation rates suggested for the interior of the MCT thrust sheet in the Chamba area (Pir Panjal range, 0.3–0.9 mm/yr, Deeken et al., 2011). These values of $\dot{\epsilon}_2$ result in geothermal gradients of ~ 20 to ~ 22 °C/km at the onset of Pliocene exhumation, which we consider reasonable estimates for a slowly exhuming central Himachal Himalaya. We ran suites of forward simulations to constrain the best-fit onset of the Pliocene exhumation stage T_3 for a given ‘initial’ thermal field (i.e., different values of $\dot{\epsilon}_2$) and given fault kinematics (ramp angle and overthrusting velocities v_3).

5.2. Model results and discussion

Fig. 6A shows a Pecube implementation of 15° dipping MHT ramp, which was active from 5.8 to 0 Ma at $v_3 = 7$ mm/yr (i.e., 50%) overthrusting. The model reproduces the observed AFT and ZHe ages (Fig. 7) and predicts MAr ages ≥ 19 Ma. Because erosion in the Chandra catchment may be restricted by low precipitation (Fig. 1D), the modelling assumption that rock uplift is fully compensated by surface denudation may not be valid there. Consequently, the northern limit of the ramp is poorly constrained by the thermochronological data, and the ramp may extend farther north. Similarly, we attribute little significance to the 10° dip of the lower part of the MHT; we chose this value because it reproduces the thermochronological data in the North Himalaya, but this conformance may be coincidental.

While a wide range of parameter combinations reproduces the ZHe and AFT ages reasonably well, few models meet the constraint that no MAr is reset after 19 Ma. The model in Fig. 6A ($\dot{\epsilon}_2 = 0.15$ mm/yr, $T_3 = 5.8$ Ma, $v_3 = 7$ mm/yr) yielded the lowest misfit of all parameter combinations ($\dot{\epsilon}_2 = 0.15$ to 0.3 mm/yr, ramp angle 10 to 20° , $v_3 = 5$ to 7 mm/yr; misfit = 40 calculated for all AFT and ZHe data). Figs. 6B–6C show average (black lines) and range of (grey bands) AFT, ZHe, and MAr ages predicted by this model as a function of distance to the MHT trace. Muscovite $^{40}\text{Ar}/^{39}\text{Ar}$ ages are ~ 20 Ma above the upper end of the MHT ramp and increase towards the northeast. Models with the same ramp dip and v_3 but with higher exhumation rates $\dot{\epsilon}_2$ reproduce the age data if the duration of S_3 is shortened: for example, Fig. 6B shows a comparison of $\dot{\epsilon}_2 = 0.15$ mm/yr, $T_3 = 5.8$ Ma (black), $\dot{\epsilon}_2 = 0.2$ mm/yr, $T_3 = 5.1$ Ma (blue), and $\dot{\epsilon}_2 = 0.3$ mm/yr, $T_3 = 4.1$ Ma (red). For all different ramp angles and slip velocities, $\dot{\epsilon}_2 = 0.3$ mm/yr yields a significantly higher misfit (≥ 130) than lower values of $\dot{\epsilon}_2$. In accordance with the 1D inversions, the ramp models suggest that between early Miocene exhumation from mid-crustal depths and the Pliocene exhumation episode there was an extended period with very low exhumation rates. We interpret the 0.3 mm/yr suggested by Deeken et al. (2011) a maximum estimate

for middle-late Miocene erosion rates in the central Himachal Himalaya.

Different combinations of ramp angles and MHT slip velocities may predict comparable patterns of erosion rates and cooling ages. For a 15° dipping ramp, the age predictions for $v_3 = 7$ mm/yr, $T_3 = 5.8$ Ma and $v_3 = 5$ mm/yr, $T_3 = 8.6$ Ma are similar, although the ZHe ages predicted by the latter model are ~ 2 Myr too old (misfit = 177; Fig. 6C, black and yellow). Steeper ramps cause higher exhumation rates above the ramp and thus predict a shorter duration of S_3 and a narrower band of Pliocene ZHe ages (e.g., Fig. 6C, green). Although the available data do not allow us to constrain the ramp geometry several general conclusions can be drawn from the modelling results. (1) High exhumation rates are required during S_3 to account for Pliocene ZHe ages over a range of elevations from ~ 1500 to 4000 m asl (Fig. 7B); 1D inversion suggests $\dot{\epsilon}_3 = 3$ mm/yr, the MHT ramp models employ $\dot{\epsilon}_3 \sim 1.5$ to 2.5 mm/yr. We estimate that Pliocene exhumation of the Beas/Tosh GHS occurred at a rate of ~ 2 –3 mm/yr. (2) Because of the high exhumation rates $\dot{\epsilon}_3$, there is a lower limit to probable ramp angles and overthrusting velocities: for example, for a 10° dipping ramp even high overthrusting velocities >7 mm/yr (i.e. $>50\%$ of total shortening) do not reproduce rapid Pliocene cooling through the ZHe closure isotherm without resetting MAr ages. (3) Variable dip of 15 – 20° and overthrusting velocities 5–7 mm/yr require onset of rapid exhumation at $T_3 \sim 4$ –7 Ma. All models suggest that rapid exhumation did not end before Present.

The low middle-late Miocene exhumation rates (<0.3 mm/yr) may be interpreted to indicate a period of tectonic quiescence. However, the MCT was active until ~ 16 Ma (Vannay et al., 2004) or ~ 10 Ma (Caddick et al., 2007), and convergence rates between India and Asia are probably constant since at least 10 Ma (Molnar and Stock, 2009). Therefore, we attribute slow middle-late Miocene exhumation to a subhorizontal MHT that did not drive significant rock uplift and erosion; before the Pliocene, the MHT geometry probably resembled Fig. 4A more than Fig. 4C. The kinematics must have changed in the late Miocene to early Pliocene with the development of a ramp in a gently dipping MHT (e.g. Mercier et al., 2017) and out-of-sequence thrusting on the MT and/or duplex formation. In the Jiwa section, it could be argued that an out-of-sequence thrust coincides with the contact between Wangtu gneiss and overlying Berinag quartzite, but the significant displacement required to explain the observed offset in ZHe ages (e.g., ~ 4 –7 Myr $\cdot 14$ mm/yr) would also offset the MCT at the NW margin of the window in contradiction with detailed mapping in this area (Thöni, 1977). Basal accretion associated with duplex formation in the LHS or the development of an MHT ramp are therefore more likely mechanism driving rapid Pliocene exhumation of the Beas/Tosh GHS.

The middle Miocene ZHe ages within the KLRW place an upper limit on the exhumation depth there: although the antiform probably experienced rapid denudation during its formation this episode must have been relatively short-lived. We propose that the KLRW antiform is caused by an LHS duplex that formed during an early stage of basal accretion, i.e., in the late Miocene to early Pliocene.

Continued thrusting on the MHT carried the duplex southward while basal accretion and rapid hanging wall exhumation continued northeast of the window. This is similar to the Sutlej section where Webb (2013) suggested that the KLRW antiform initiated as a fault-ramp fold in the middle Miocene and was subsequently transported southwards and exhumed by continued basal accretion of LHS horses.

The Bajaura unit in the western window is folded by the KLRW antiform. If the KLRW antiform formed in the late Miocene to early Pliocene, ductile shear in the Bajaura unit must have ended in the late Miocene or earlier. This is thus indistinguishable from estimates of MCT deformation, which may have continued until ~10 Ma (Caddick et al., 2007). Following Stephenson et al. (2001), we argue that the Bajaura ‘nappe’ is part of the MCT shear zone, a distinct protolith within a kilometre-wide mylonite belt; thrusting within the Bajaura unit and the MCT shear zone occurred from 26–23 Ma to the middle-late Miocene, either continuously or episodically. The correlation of the RMT across the Himalaya remains a matter of debate. In the Garhwal and Nepal Himalaya, the Ramgarh thrust sheet is described as a 2–3 km thin section below the MCT, which is discriminated from the MCT shear zone mostly based on the different lithologies of the two thrust sheets (Ramgarh thrust sheet = LHS; MCT sheet = GHS; Pearson and DeCelles, 2005; Robinson and Pearson, 2013). This is similar to the description of the Bajaura unit and MCT shear zone in Kishtwar (Stephenson et al., 2001) suggesting that the RMT may extend as far west as the Kishtwar region. This hypothesis is supported by similar middle Miocene age estimates for shear on the Ramgarh thrust in Nepal (Pearson and DeCelles, 2005; Kohn et al., 2004) and in the Kishtwar area (deformation ~23–15 Ma within the combined MCT and Bajaura shear zone progressively cutting down-section; Stephenson et al., 2001). The late Miocene–Pliocene age of the MT in the Sutlej section (Vannay et al., 2004; Caddick et al., 2007) is significantly younger. We demonstrated that the MT as described in the Sutlej section terminates laterally in central Himachal Pradesh. If the Bajaura unit is to be correlated with the Ramgarh thrust sheet, the geometric relationships in central Himachal Pradesh suggest that this orogen-wide shear zone is a complex structure consisting of at least two en échelon faults, the MT and a shear zone at the base of the Bajaura unit. Similar complexities may exist in the central and eastern Himalaya, and may account for different ages of shear along segments of the RMT.

6. Synthesis and conclusions

Published maps of the western Kullu–Larji–Rampur window (KLRW) suggest a variety of geometries for the Munsiri thrust (MT) west of the Sutlej section. For example, the MT has been interpreted as a blind-fault and the KLRW antiform as a fault-propagation fold above the MT (e.g., Vannay and Grasemann, 2001). Alternatively, the Bajaura nappe, which has been mapped along the northern, western, and southwestern window margin has been correlated with the MT sheet (the ‘Lesser Himalayan crystalline’) in the eastern KLRW, implying that both the MT and MCT are folded by the KLRW antiform (e.g., Steck, 2003). Our mapping of the ~1 km thick sequence of graphitic schists and mylonitic augen gneiss of the Bajaura unit along the northeastern margin of the window suggests that this unit is part of the MCT shear zone (Stephenson et al., 2001). The MT was not unambiguously identified in the western window; the contacts between the Wangtu orthogneiss and the overlying and underlying Berinag quartzite are tectonic contacts, but a prominent mylonitic shear zone comparable to the MT in the Sutlej section was not observed. Our observations do not contradict models of the MT located at the base of the Wangtu gneiss (e.g., Webb et al., 2011), nor can we rule out the possibility that the MT is a blind thrust below the central

Himachal GHS northeast of the window (Vannay and Grasemann, 2001). In either case, there is no evidence for the MT west of the KLRW.

The exhumation history of the central Himachal Himalaya is episodic. In the late Oligocene to early Miocene, thrusting along the MCT exhumed the GHS rapidly from ~20–30 km to shallow-crustal depth leading to cooling below the muscovite $^{40}\text{Ar}/^{39}\text{Ar}$ closure temperature by ~20–21 Ma (e.g., Schlup et al., 2011; Stübner et al., 2014). Here we show that middle-late Miocene exhumation rates in the central Himachal Himalaya were <0.3 mm/yr. Because the MCT was probably active until ~16–10 Ma, these low exhumation rates are attributed to a shallow dip of the MCT. The periodicity of exhumation is not caused by unsteady shortening rates but by the passage of material points over ramp and flat segments of the basal detachment resulting in variable rock uplift rate in space and time.

We suggest that a ramp formed in the basal thrust of the orogenic wedge (MHT) in the late Miocene to early Pliocene leading to the development of an LHS duplex and the KLRW antiform. Rapid exhumation above this ramp is reflected in a ~40 km wide belt of Pliocene zircon (U–Th)/He ages northeast of the KLRW. Although the LHS rocks in the northwestern part of the KLRW are probably also affected by the Pliocene exhumation episode, zircon (U–Th)/He ages in the Wangtu orthogneiss are mid-Miocene and older suggesting that (a) Pliocene exhumation depths in the northwestern KLRW are shallower compared to the GHS and (b) because of the shallow dip of the MCT in the mid-Miocene, LHS rocks were not heated sufficiently during underthrusting to fully reset the zircon (U–Th)/He system. We estimate an onset of rapid exhumation at ~4–7 Ma and exhumation rates ~2–3 mm/yr; rapid exhumation may be ongoing. The belt of rapid Pliocene exhumation in the central Himachal Himalaya coincides with the exposure of amphibolite-facies GHS rocks. The spatial distribution of metamorphic GHS rocks in the northwestern Himalaya (see Fig. 1A) may thus be primarily controlled by Pliocene tectonics. This belt of rapid Pliocene exhumation continues eastward in the eastern Himachal and Garhwal Himalaya (Thiede et al., 2009).

We speculate that the northwest Himalayan MCT shear zone comprising the sheared basal sections of the Haimanta metasediments (GHS) and the Bajaura ‘nappe’ (LHS) is equivalent to the MCT and Ramgarh thrust sheet in Nepal and Garhwal Himalaya (Pearson and DeCelles, 2005; Robinson and Pearson, 2013). Deformation on the MCT and within the Bajaura unit probably occurred from the early to middle-late Miocene progressively downcutting with time (Stephenson et al., 2001). These estimates are comparable to age of the MCT (early Miocene) and Ramgarh thrust sheet (middle Miocene) in Nepal (Pearson and DeCelles, 2005). In contrast, the late Miocene–Pliocene age of the Himachal MT (Sutlej section and probably also Beas section) is ~5 Myr younger than the latest shear within the Bajaura and Ramgarh thrust sheets. The MT sheet and Bajaura ‘nappe’ are mapped as separate units, and the MT terminates laterally in central Himachal Pradesh. This suggests that although the RMT may be an orogen-scale structure traceable as far west 75°E, it appears to be a complex structure consisting of several segments the geometry and age of which vary along the orogen.

Acknowledgements

This study is funded by the German Science Foundation grant STU 525/1-1 to K.S. and by the Excellence Initiative of University of Tübingen (grant to K.S.). Fieldwork was supported by the Natural Sciences and Engineering Research Council of Canada (discovery grant RGPIN 04297 to D.G.). We thank Todd Ehlers for financial support. Jean Braun provided access to Pecube software. We are indebted to Tashi Tsering and Talat Ahmat for their assistance with

field work in the Himachal Himalaya. K.S. acknowledges inspiring discussions with Paul Bons. Comments by Peter van der Beek and an anonymous reviewer improved an earlier version of this manuscript, and we acknowledge their reviews and editorial handling by An Yin.

Appendix A. Supplementary material

Supplementary material related to this article can be found online at <https://doi.org/10.1016/j.epsl.2017.10.036>.

References

- Allmendinger, R.W., 1998. Inverse and forward numerical modelling of trishear fault-propagation folds. *Tectonics* 17 (4), 640–656.
- Bollinger, L., Henry, P., Avouac, J.P., 2006. Mountain building in the Nepal Himalaya: thermal and kinematic model. *Earth Planet. Sci. Lett.* 244 (1), 58–71. <https://doi.org/10.1016/j.epsl.2006.01.045>.
- Bookhagen, B., Burbank, D.W., 2010. Toward a complete Himalayan hydrological budget: spatiotemporal distribution of snowmelt and rainfall and their impact on river discharge. *J. Geophys. Res., Earth Surf.* 115 (F3). <https://doi.org/10.1029/2009JF001426>.
- Braun, J., Van Der Beek, P., Valla, P., Robert, X., Herman, F., Glotzbach, C., Pedersen, V., Perry, C., Simon-Labric, T., Prigent, C., 2012. Quantifying rates of landscape evolution and tectonic processes by thermochronology and numerical modelling of crustal heat transport using PECUBE. *Tectonophysics* 524, 1–28. <https://doi.org/10.1016/j.tecto.2011.12.035>.
- Caddick, M.J., Bickle, M.J., Harris, N.B.W., Holland, T.J.B., Horstwood, M.S.A., Parrish, R.R., Ahmad, T., 2007. Burial and exhumation history of a Lesser Himalayan schist: recording the formation of an inverted metamorphic sequence in NW India. *Earth Planet. Sci. Lett.* 264 (3), 375–390. <https://doi.org/10.1016/j.epsl.2007.09.011>.
- Caldwell, W.B., Klempner, S.L., Lawrence, J.F., Rai, S.S., 2013. Characterizing the Main Himalayan Thrust in the Garhwal Himalaya, India with receiver function CCP stacking. *Earth Planet. Sci. Lett.* 367, 15–27. <https://doi.org/10.1016/j.epsl.2013.02.009>.
- Célérier, J., Harrison, T.M., Beyssac, O., Herman, F., Dunlap, W.J., Webb, A.A.G., 2009. The Kumaon and Garhwal Lesser Himalaya, India: Part 2. Thermal and deformation histories. *Geol. Soc. Am. Bull.* 121 (9–10), 1281–1297. <https://doi.org/10.1130/B26343.1>.
- Coutand, I., Whipp, D.M., Grujic, D., Bernet, M., Fellin, M.G., Bookhagen, B., Landry, K.R., Ghalley, S.K., Duncan, C., 2014. Geometry and kinematics of the Main Himalayan Thrust and Neogene crustal exhumation in the Bhutanese Himalaya derived from inversion of multithermochronologic data. *J. Geophys. Res., Solid Earth* 119 (2), 1446–1481. <https://doi.org/10.1002/2013JB010891>.
- Deeken, A., Thiede, R.C., Sobel, E.R., Hourigan, J.K., Strecker, M.R., 2011. Exhumational variability within the Himalaya of northwest India. *Earth Planet. Sci. Lett.* 305 (1), 103–114. <https://doi.org/10.1016/j.epsl.2011.02.045>.
- Epard, J.L., Steck, A., Vannay, J.C., Hunziker, J.C., 1995. Tertiary Himalayan structures and metamorphism in the Kulu Valley (Mandi-Khokras transect of the Western Himalaya) – Shikar-Beh-nappe and crystalline nappe. *Schweiz. Mineral. Petrogr. Mitt.* 75, 59–84. <https://doi.org/10.5169/seals-57144>.
- Frank, W., Grasemann, B., Guntli, P., Miller, C., 1995. Geological map of the Kishtwar-Chamba-Kulu region (NW Himalayas, India). *Jahrb. Geol. Bundesanst.* 138 (2), 299–308.
- Grasemann, B., 1993. Numerical modelling of the thermal history of the NW Himalayas, Kulu Valley, India. *Geol. Soc. (Lond.) Spec. Publ.* 74 (1), 475–484.
- Herman, F., Copeland, P., Avouac, J.P., Bollinger, L., Mahéo, G., Le Fort, P., Rai, S., Foster, D., Pécher, A., Stüwe, K., Henry, P., 2010. Exhumation, crustal deformation, and thermal structure of the Nepal Himalaya derived from the inversion of thermochronological and thermobarometric data and modelling of the topography. *J. Geophys. Res., Solid Earth* 115 (B6). <https://doi.org/10.1029/2008JB006126>.
- Hollister, L.S., Grujic, D., 2006. Pulsed channel flow in Bhutan. *Geol. Soc. (Lond.) Spec. Publ.* 268 (1), 415–423. <https://doi.org/10.1144/GSL.SP.2006.268.01.19>.
- Jade, S., Mukul, M., Gaur, V.K., Kumar, K., Shringeshwar, T.S., Satyal, G.S., Dumka, R.K., Jagannathan, S., Ananda, M.B., Kumar, P.D., Banerjee, S., 2014. Contemporary deformation in the Kashmir–Himachal, Garhwal and Kumaon Himalaya: significant insights from 1995–2008 GPS time series. *J. Geod.* 88 (6), 539–557. <https://doi.org/10.1007/s00190-014-0702-3>.
- Jain, A.K., Anand, A., 1988. Deformational and strain patterns of an intracontinental collision ductile shear zone – an example from the Higher Garhwal Himalaya. *J. Struct. Geol.* 10 (7), 717–734. [https://doi.org/10.1016/0191-8141\(88\)90079-X](https://doi.org/10.1016/0191-8141(88)90079-X).
- Jain, A.K., Kumar, D., Singh, S., Kumar, A., Lal, N., 2000. Timing, quantification and tectonic modelling of Pliocene–Quaternary movements in the NW Himalaya: evidence from fission track dating. *Earth Planet. Sci. Lett.* 179 (3), 437–451.
- Kohn, M.J., Wieland, M.S., Parkinson, C.D., Upreti, B.N., 2004. Miocene faulting at plate tectonic velocity in the Himalaya of central Nepal. *Earth Planet. Sci. Lett.* 228 (3), 299–310. <https://doi.org/10.1016/j.epsl.2004.10.007>.
- Larson, K.P., Godin, L., 2009. Kinematics of the Greater Himalayan sequence, Dhaulagiri Himal: implications for the structural framework of central Nepal. *J. Geol. Soc.* 166 (1), 25–43. <https://doi.org/10.1144/0016-76492007-180>.
- Law, R.D., Stahr, D.W., Francis, M.K., Ashley, K.T., Grasemann, B., Ahmad, T., 2013. Deformation temperatures and flow vorticities near the base of the Greater Himalayan Series, Sutlej Valley and Shimla Klippe, NW India. *J. Struct. Geol.* 54, 21–53. <https://doi.org/10.1016/j.jsg.2013.05.009>.
- Long, S.P., McQuarrie, N., Tobgay, T., Grujic, D., 2011. Geometry and crustal shortening of the Himalayan fold-thrust belt in Bhutan. *Geol. Soc. Am. Bull.* 123, 1427–1447. <https://doi.org/10.1130/B30203.1>.
- Mandal, S., Robinson, D.M., Khanal, S., Das, O., 2014. Redefining the tectonostratigraphic and structural architecture of the Almora klippe and the Ramgarh–Munsiari thrust sheet in NW India. *Geol. Soc. (Lond.) Spec. Publ.* 412 (1), 247–269. <https://doi.org/10.1144/SP412.6>.
- Meigs, A.J., Burbank, D.W., Beck, R.A., 1995. Middle-late Miocene (>10 Ma) formation of the Main Boundary thrust in the western Himalaya. *Geology* 23 (5), 423–426. [https://doi.org/10.1130/0091-7613\(1995\)023<0423:MLMMFO>2.3.CO;2](https://doi.org/10.1130/0091-7613(1995)023<0423:MLMMFO>2.3.CO;2).
- Mercier, J., Braun, J., van der Beek, P., 2017. Do along-strike tectonic variations in the Nepal Himalaya reflect different stages in the accretion cycle? Insights from numerical modeling. *Earth Planet. Sci. Lett.* 472, 299–308. <https://doi.org/10.1016/j.epsl.2017.04.041>.
- Miller, C., Klötzli, U., Frank, W., Thöni, M., Grasemann, B., 2000. Proterozoic crustal evolution in the NW Himalaya (India) as recorded by circa 1.80 Ga mafic and 1.84 Ga granitic magmatism. *Precambrian Res.* 103 (3), 191–206. [https://doi.org/10.1016/S0301-9268\(00\)00091-7](https://doi.org/10.1016/S0301-9268(00)00091-7).
- Molnar, P., Stock, J.M., 2009. Slowing of India's convergence with Eurasia since 20 Ma and its implications for Tibetan mantle dynamics. *Tectonics* 28 (3). <https://doi.org/10.1029/2008TC002271>.
- Montomoli, C., Carosi, R., Iaccarino, S., 2015. Tectonometamorphic discontinuities in the Greater Himalayan Sequence: a local or a regional feature? *Geol. Soc. (Lond.) Spec. Publ.* 412 (1), 25–41. <https://doi.org/10.1144/SP412.3>.
- Pearson, O.N., DeCelles, P.G., 2005. Structural geology and regional tectonic significance of the Ramgarh thrust, Himalayan fold-thrust belt of Nepal. *Tectonics* 24 (4). <https://doi.org/10.1029/2003TC001617>.
- Powers, P.M., Lillie, R.J., Yeats, R.S., 1998. Structure and shortening of the Kangra and Dehra Dun reentrants, sub-Himalaya, India. *Geol. Soc. Am. Bull.* 110 (8), 1010–1027. [https://doi.org/10.1130/0016-7606\(1998\)110<1010:SASOTK>2.3.CO;2](https://doi.org/10.1130/0016-7606(1998)110<1010:SASOTK>2.3.CO;2).
- Robert, X., Van Der Beek, P., Braun, J., Perry, C., Mugnier, J.L., 2011. Control of detachment geometry on lateral variations in exhumation rates in the Himalaya: insights from low-temperature thermochronology and numerical modelling. *J. Geophys. Res., Solid Earth* 116 (B5). <https://doi.org/10.1029/2010JB007893>.
- Robinson, D.M., McQuarrie, N., 2012. Pulsed deformation and variable slip rates within the central Himalayan thrust belt. *Lithosphere* 4 (5), 449–464. <https://doi.org/10.1130/L204.1>.
- Robinson, D.M., Pearson, O.N., 2013. Was Himalayan normal faulting triggered by initiation of the Ramgarh–Munsiari thrust and development of the Lesser Himalayan duplex? *Int. J. Earth Sci.* 102 (7), 1773–1790. <https://doi.org/10.1007/s00531-013-0895-3>.
- Robyr, M., Hacker, B.R., Mattinson, J.M., 2006. Doming in compressional orogenic settings: new geochronological constraints from the NW Himalaya. *Tectonics* 25 (2). <https://doi.org/10.1029/2004TC001774>.
- Schlup, M., Steck, A., Carter, A., Cosca, M., Epard, J.L., Hunziker, J., 2011. Exhumation history of the NW Indian Himalaya revealed by fission track and ⁴⁰Ar/³⁹Ar ages. *J. Asian Earth Sci.* 40 (1), 334–350. <https://doi.org/10.1016/j.jseas.2010.06.008>.
- Searle, M.P., Law, R.D., Godin, L., Larson, K.P., Streule, M.J., Cottle, J.M., Jessup, M.J., 2008. Defining the Himalayan main central thrust in Nepal. *J. Geol. Soc.* 165 (2), 523–534. <https://doi.org/10.1144/0016-76492007-081>.
- Srivastava, P., Mitra, G., 1994. Thrust geometries and deep structure of the outer and lesser Himalaya, Kumaon and Garhwal (India): implications for evolution of the Himalayan fold-and-thrust belt. *Tectonics* 13 (1), 89–109.
- Steck, A., 2003. Geology of the NW Indian Himalaya. *Eclogae Geol. Helv.* 96 (2), 147. <https://doi.org/10.1007/s00015-003-1091-4>.
- Stephenson, B.J., 1997. The Tectonic and Metamorphic Evolution of the Main Central Thrust Zone and High Himalaya Around the Kishtwar and Kulu Windows, Northwest India. PhD thesis. Oxford University, Oxford.
- Stephenson, B.J., Searle, M.P., Waters, D.J., Rex, D.C., 2001. Structure of the Main Central Thrust zone and extrusion of the High Himalayan deep crustal wedge, Kishtwar–Zaskar Himalaya. *J. Geol. Soc.* 158 (4), 637–652. <https://doi.org/10.1144/jgs.158.4.637>.
- Stevens, V.L., Avouac, J.P., 2015. Interseismic coupling on the main Himalayan thrust. *Geophys. Res. Lett.* 42 (14), 5828–5837. <https://doi.org/10.1002/2015GL064845>.
- Stübner, K., Grujic, D., Parrish, R.R., Roberts, N.M., Kronz, A., Wooden, J., Ahmad, T., 2014. Monazite geochronology unravels the timing of crustal thickening in NW Himalaya. *Lithos* 210, 111–128. <https://doi.org/10.1016/j.lithos.2014.09.024>.
- Stübner, K., Warren, C., Ratschbacher, L., Sperner, B., Kleeberg, R., Pfänder, J., Grujic, D., 2017. Anomalously old biotite ⁴⁰Ar/³⁹Ar ages in the NW Himalaya. *Lithosphere* 9, 366–383. <https://doi.org/10.1130/L586.1>.

- Thiede, R.C., Arrowsmith, J.R., Bookhagen, B., McWilliams, M.O., Sobel, E.R., Strecker, M.R., 2005. From tectonically to erosionally controlled development of the Himalayan orogen. *Geology* 33 (8), 689–692. <https://doi.org/10.1130/G21483.1>.
- Thiede, R.C., Ehlers, T.A., Bookhagen, B., Strecker, M.R., 2009. Erosional variability along the northwest Himalaya. *J. Geophys. Res., Earth Surf.* 114 (F1). <https://doi.org/10.1029/2008JF001010>.
- Thiede, R.C., Robert, X., Stübner, K., Dey, S., Faruhn, J., 2017. Sustained out-of-sequence shortening along a tectonically active segment of the Main Boundary Thrust: the Dhauladhar Range in the NW Himalaya. *Lithosphere* 9 (5), 715–725. <https://doi.org/10.1130/L630.1>.
- Thöni, M., 1977. *Geology, structural evolution and metamorphic zoning in the Kulu Valley (Himachal Himalayas, India) with special reference to the reversed metamorphism*. Mitt. Ges. Geol. Bergbaustud. Österr. 24.
- Vannay, J.C., Grasemann, B., 2001. Himalayan inverted metamorphism and syn-convergence extension as a consequence of a general shear extrusion. *Geol. Mag.* 138 (03), 253–276.
- Vannay, J.C., Grasemann, B., Rahn, M., Frank, W., Carter, A., Baudraz, V., Cosca, M., 2004. Miocene to Holocene exhumation of metamorphic crustal wedges in the NW Himalaya: evidence for tectonic extrusion coupled to fluvial erosion. *Tectonics* 23 (1). <https://doi.org/10.1029/2002TC001429>.
- Webb, A.A.G., 2013. Preliminary balanced palinspastic reconstruction of Cenozoic deformation across the Himachal Himalaya (northwestern India). *Geosphere* 9 (3), 572–587. <https://doi.org/10.1130/GES00787.1>.
- Webb, A.A.G., Yin, A., Harrison, T.M., Célérier, J., Gehrels, G.E., Manning, C.E., Grove, M., 2011. Cenozoic tectonic history of the Himachal Himalaya (northwestern India) and its constraints on the formation mechanism of the Himalayan orogen. *Geosphere* 7 (4), 1013–1061. <https://doi.org/10.1130/GES00627.1>.
- Whipp, D.M., Ehlers, T.A., Blythe, A.E., Huntington, K.W., Hodges, K.V., Burbank, D.W., 2007. Plio-Quaternary exhumation history of the central Nepalese Himalaya: 2. Thermokinematic and thermochronometer age prediction model. *Tectonics* 26 (3). <https://doi.org/10.1029/2006TC001991>.
- Wyss, M., 2000. Metamorphic evolution of the northern Himachal Himalaya: phase equilibria constraints and thermobarometry. *Schweiz. Mineral. Petrogr. Mitt.* 80 (3), 317–350.